Engineering active sites on binary metal selenide heterointerface catalyst to boost urea electrooxidation

Felix Ofori Boakye [a,b,*], Marshet Getaye Sendeku [c,**], Anuj Kumar [d,**], Saira Ajmal [a,b], Kwadwo Asare Owusu [a,b], Kassa Belay Ibrahim [e], Mohammad Tabish [f], Fakhr uz Zaman [a,b], Muhammad Asim Mushtaq [a], Khalid M. Alotaibi [g], Mohd Zahid Ansari [h], Ghulam Yasin [i,j,***]

[a] *Institute for Advanced Study, Shenzhen University, Shenzhen 518060, China*
[b] *College of Physics and Optoelectronic Engineering, Shenzhen University, Shenzhen 518060, China*
[c] *Ocean Hydrogen Energy R&D Center, Research Institute of Tsinghua University in Shenzhen, Shenzhen, China*
[d] *Nano-Technology Research Laboratory, Department of Chemistry, GLA University, Mathura, Uttar Pradesh 281406, India*
[e] *Department of Molecular Sciences and Nanosystems, Ca' Foscari University of Venice, Via Torino 155, Venezia, Mestre 30172, Italy*
[f] *College of Materials Science and Engineering, Beijing University of Chemical Technology, Beijing 100029, China*
[g] *Department of Chemistry, King Saud University, Riyadh 11451, Saudi Arabia*
[h] *School of Materials Science and Engineering, Yeungnam University, 280 Daehak-Ro, Gyeongsan, Gyeongbuk 38541, Republic of Korea*
[i] *School of Environment and Civil Engineering, Dongguan University of Technology, Dongguan, Guangdong 523808, China*
[j] *School of Environmental Science and Engineering, Tianjin University, Tianjin 300350, China*

ARTICLE INFO

ABSTRACT

Electrocatalytic urea oxidation reaction (UOR) with a low thermodynamic potential is a perfect substitute for anodic oxygen evolution process (OER) in the effective generation of hydrogen. However, because of the slow kinetics of UOR, its potential application for commercial use remains untapped. Nickel-based materials may be an option for urea oxidation reaction but the heavily filled d orbital prevents enhanced adsorption and activity. Here, taking into account the adsorption-energy scaling limitations, Co^{3+} with partially filled d orbital is introduced into nickel selenide to form a heterointerface catalyst (2D CoSe$_2$/Ni$_{0.85}$Se) that enhances UOR. As anticipated, the 2D CoSe$_2$/Ni$_{0.85}$Se electrode displays a low potential of 1.33 V to achieve 100 mA cm^{-2} for UOR while retaining strong durability for 300 h. Further, 2D CoSe$_2$/Ni$_{0.85}$Se catalyst is used as an anode in an anion exchange membrane flow electrolyzer, which achieved an industrial-level voltage of 1.91 V at 1 A cm^{-2} and robust durability.

1. Introduction

The generation of renewable hydrogen (H$_2$) from water electrolysis has been suggested as a potential remedy to mitigate the energy crisis and environmental problems [1–4]. Nevertheless, this electrochemical process for large-scale generation of H$_2$ cannot meet the global demand for H$_2$ due to the high cost needed to drive the kinetically sluggish oxygen evolution reaction (OER) [5–7]. Urea oxidation reaction (UOR) is industrially significant for the construction of renewable energy systems mainly because of their lower thermodynamic potential when compared with oxygen evolution reaction (0.37 V vs 1.23 V) for high-purity H$_2$ in energy conversion devices [8–11]. Moreover, urea is universally available in human urine, industrial and sanitary wastewater which makes its electrolysis more feasible [12,13]. Nonetheless, the major challenges associated with the 6e- transfer UOR, the slow kinetics, complicated intermediate species, and high overpotential severely impede its practical use [14,15].

Noble metal catalysts including Ru-TiO$_2$ and Ti-Pt have proven to be excellent electrocatalysts for UOR, but their low durability, high cost, and restricted availability prevent them from being used widely [16].

---

* Corresponding author at: Institute for Advanced Study, Shenzhen University, Shenzhen 518060, China.
** Corresponding authors.
*** Corresponding author at: School of Environment and Civil Engineering, Dongguan University of Technology, Dongguan, Guangdong 523808, China.
E-mail addresses: felix88@whut.edu.cn (F.O. Boakye), marshet@Tsinghua-sz.org (M.G. Sendeku), anuj.kumar@gla.ac.in (A. Kumar), yasin.bzu@hotmail.com, yasin@mail.buct.edu.cn (G. Yasin).

Hence, searching for high-performance catalysts for UOR is highly desired for attaining large-scale hydrogen production in energy-saving water electrolyzers. Recently, various earth-abundant materials such as Ni-based materials have been recognized as potential candidates for urea water electrolysis. Ni-based materials such as oxides [17,18], sulfides [19,20], selenides [21,22], and nitrides [23] have been developed with enhanced performance for UOR. Among these, nickel selenide is identified as a promising catalyst for UOR [24]. To enhance the activity of this catalyst, different approaches, including morphological engineering, defect engineering, and heterostructure engineering have been used in this research field [25]. The utilization of different nanostructures through material synthesis can enhance the performance of electrocatalysts. For example, $Ni_3Se_4/NiSe_2$ rod-like nanoarrays [26], and $NiSe_2$ nanoparticle/NiO nanosheets [27] have been fabricated for superior UOR. In addition, heterostructure engineering allows for the broad fabrication of hybrids using a variety of transition-metal electrocatalysts, controlling electron transport and performance due to the creation of coupling interfaces and the synergistic effects of the formed heterostructures. For example, numerous heterostructures including $NiSe_2/MoSe_2$ [28], Ni-TPA@NiSe/NF [29], and $NiSe_2$-$NiMoO_4$ [9] have been fabricated and investigated.

However, the catalytic activity of nickel selenide is still unsatisfactory in alkaline electrolytes, which is due to the poor adsorption capacity of Ni sites toward UOR reactants, which makes it difficult to follow dissociation steps [30]. The insufficient catalytic activity may be caused by the Ni^{2+} sites in nickel selenide with a densely packed d orbital ($3d^8$) interacting poorly with water or urea molecules oxygen atoms [31]. It is challenging to balance the energies in nickel selenides with single-Ni active sites because of the intrinsic scaling connection of adsorption energies within reaction intermediates [32]. Hence, the addition of different sites with strong interaction with oxygen atoms to design a heterointerface catalyst is sought to be an efficient approach to break through the adsorption-energy scaling limitations and enhance the catalytic activity of nickel selenides towards UOR. An effective method for overcoming the aforementioned issues with transition metal selenide catalysts is heterostructure engineering. This is because the heterostructure interfaces that are created can produce favorable electronic characteristics, such as optimized adsorption energy from charge redistribution and enhanced active site from lattice mismatch, and defects [33–36]. Currently, $CoSe_2$ has been suggested as a prospective electrocatalyst promoter because of its distinctive properties, such as the provision of active sites to adsorb urea molecules and its excellent durability. Hence, designing cost-efficient heterointerface catalysts is essential to enhance reaction kinetics for UOR and also promote the efficiency of energy conversion devices.

Here, we designed a 2D $CoSe_2/Ni_{0.85}Se$ heterostructure catalyst through a feasible hydrothermal technique for efficient UOR catalysis. The electronic coupling between the $CoSe_2$ and $Ni_{0.85}Se$ can initiate enhanced activity for UOR and this is due to the robust electronic interaction between metal cations and selenide. Moreover, the 2D $CoSe_2/Ni_{0.85}Se$ catalyst electrode displays a very low potential of 1.33 V and strong stability for more than 300 h at 100 mA cm^{-2}. Theoretical calculations show that a 2D $CoSe_2/Ni_{0.85}Se$ heterostructure catalyst optimizes the adsorption/desorption energy of the intermediates by decreasing the Gibbs free energy barrier of each step in UOR. Additionally, adopting 2D $CoSe_2/Ni_{0.85}Se$ as the anode for a single-cell AEM urea electrolyzer enables this electrode to attain a current density of 1 A cm^{-2} at a voltage of 1.91 V while retaining robust durability for potential industrial applications. This study provides insights into the development of effective catalysts for urea oxidation reactions for the generation of hydrogen (H_2).

2. Experimental section

2.1. Materials and chemicals

Sinopharm Chemical Reagent Company in China was the source of the following supplies: nickel (II) nitrate hexahydrate, cobalt nitrate hexahydrate, urea, ammonium fluoride (NH_4F), and ethanol. We bought powdered selenium (Se) from Aladin Reagent in China. The chemical reagent company Sigma-Aldrich was the source of Pt/C (20 wt%) and Nafion (5 wt%). We utilized all of the other reagents we obtained without purifying them further. Deionized water that has been refined using a millipore system served as the solvent.

2.2. Preparation of Co(OH)F/Ni(OH)$_2$ on nickel foam

In this experiment, acetone, 3 M HCl, ethanol, and deionized water were used to wash a 2*4 cm piece of nickel foam in an ultrasonic bath. Subsequently, the pre-treated nickel foam's weight was determined. Co(OH)F/Ni(OH)$_2$ was synthesized using the following procedures. To create a homogeneous solution, 2 mmol of $Ni(NO_3)_2.6H_2O$, 2 mmol of $Co(NO_3)_2.6H_2O$, and 8 mmol of urea were combined with 40 ml of distilled water. Subsequently, 4 mmol of NH_4F was introduced into the homogenous mixture and stirred for 20 mins. The uniform mixture, together with the nickel foam that had been pre-treated, was put into an autoclave made of stainless steel. The autoclave was preheated for 7 h at 120 ºC in an oven. After the autoclave cooled down, Co(OH)F/Ni(OH)$_2$-NF was treated with deionized water and dried in a vacuum oven set at 60 ºC.

2.3. Preparation of 2D CoSe$_2$/Ni$_{0.85}$Se nanoplates on nickel foam

Next, using a hydrothermal process, the Co(OH)F/Ni(OH)$_2$-NF was immersed in a solution that included 0.5714 g of NaOH and 0.05 g of selenium powder in 35 ml of deionized water. After that, the hydrothermal process ran for 20 h at 180 °C. The resultant $CoSe_2/Ni_{0.85}Se$ catalyst was dried in an oven at 60 °C after being cleaned with deionized water and ethanol. The finished product was designated as 2D $CoSe_2/Ni_{0.85}Se$. The prepared 2D $CoSe_2/Ni_{0.85}Se$ on NF has a mass loading of 1.1 mg cm^{-2}. For comparison, commercial RuO_2 on NF was coated with the same mass loading (1.1 mg cm^{-2}) as 2D $CoSe_2/Ni_{0.85}Se$.

2.4. Characterizations

The material's chemical phase was determined by X-ray photoelectron spectroscopy utilizing a monochromatized A1 kα excitation and a PerkinElmer PHI 5000 C instrument. The JEOL JEM-F200 TEM equipment was utilized to evaluate the microstructure and EDS mapping images using transmission electron microscopy. The measurement of the crystalline structure of materials was accomplished by X-ray diffraction images captured using a Rigaku model Dmax/Ultima IV diffractometer using monochromatized Cu kα radiation (λ=0.15418). Elemental analysis was conducted with inductively coupled plasma-atomic emission spectroscopy (ICP-AES).

2.5. Electrochemical measurements

In a three-electrode setup, the electrochemical evaluation of this study was examined for UOR and OER in 1 M KOH with and without 0.5 M urea utilizing an electrochemical workstation (CHI 660E). 2D $CoSe_2/Ni_{0.85}Se$ and other control materials were applied as working electrodes, graphite rod, and Hg/HgO were used as counter electrodes and reference electrodes, respectively. Using the Nernst equation, the measured potentials were transformed into reversible hydrogen electrodes (RHE). Prior to testing the linear voltammetry, the working electrode was subjected to many cyclic voltammetry scans at a rate of 100 mV/s. Linear sweep voltammetry was used to construct the

polarization curves at a scanning rate of 5 mV/s. Additionally, the electrochemical stability was examined using continuous CV curves for 2000 cycles, and a 5 mV/s scanning rate was used to quickly construct the polarization curve. To evaluate the stability of 2D $CoSe_2/Ni_{0.85}Se$, the chronopotentiometry test was examined at 100 mA cm^{-2} for 300 h.

3. Results and discussion

3.1. Physicochemical characterization

To fabricate 2D $CoSe_2/Ni_{0.85}Se$ on nickel foam (NF) substrate, a two-step hydrothermal approach was employed, as displayed in Fig. 1a. Initially, $Co(OH)F$-$Ni(OH)_2$ was directly grown on a NF via hydrothermal technique with Co^{2+} and Ni^{2+} serving as the metal cations source. Next, the obtained $Co(OH)F$-$Ni(OH)_2/NF$ was added into a prepared NaHSe solution for hydrothermal reaction to synthesize $CoSe_2/Ni_{0.85}Se$ heterostructure. The X-ray diffraction (XRD) pattern was applied to study the crystallographic structures of the synthesized catalysts. As displayed in Fig. S1, the XRD pattern of $Co(OH)F/Ni(OH)_2$ exhibited two distinct phases $Co(OH)F$ (JCPDS 050-0827) and $Ni(OH)_2$ (JCPDS 014-0117). The XRD pattern of as-obtained 2D $CoSe_2/Ni_{0.85}Se$, $CoSe_2$, and $Ni_{0.85}Se$ are illustrated in Fig. 2a. The XRD peaks at 34.2°, 38.6°, 52° and 58.8°, which corresponds to (210), (211), (311), and (321) planes of cubic phase $CoSe_2$ (JCPDS 09-0234) [37] are seen along with $Ni_{0.85}Se$ peaks at 33.3°, 44.7°, 51.2° and 50.3° which correspond to (101), (102), (110) and (103) planes of hexagonal phase $Ni_{0.85}Se$ (JCPDS 018-0888) [38], suggesting the formation of heterostructures. The morphology of $Co(OH)F$-$Ni(OH)_2$ was investigated with scanning electron microscopy (SEM) and it showed a nanoplate structure (Fig. S2). The structure of 2D $CoSe_2/Ni_{0.85}Se$ was assessed with SEM and transmission electron microscopy (TEM), in which a plate-like structure of 2–5 µm lateral size is exhibited (Fig. 1b-c and S3).

Note that the hydrothermally grown $Ni_{0.85}Se$ and $CoSe_2$ show nanosheet and nanorod morphology which cover the entire substrate, respectively (Fig. S4 and S5). The TEM of $Ni_{0.85}Se$ and $CoSe_2$ were also investigated and the nanosheet and nanorods structures are confirmed from their respective characterizations (Fig. S6a-b and S7a-b). The EDS mapping of $Ni_{0.85}Se$ (Fig. S6c) displays a uniform distribution of Ni and Se over the entire sheet. Similarly, the $CoSe_2$ (Fig. S7c) nanorod shows the uniform distribution of Co and Se. The HR-TEM of the as-constructed $CoSe_2/Ni_{0.85}Se$ exhibited lattice fringes of 0.239 and 0.27 nm (Fig. 1d) which matches well with the (211) and (101) planes of $CoSe_2$ and $Ni_{0.85}Se$, respectively, further depicting the formation of the heterostructure. The related energy-dispersive X-ray (EDS) elemental mapping images exhibit the uniform dispersion of Co, Ni, and Se throughout the entire plate (Fig. 1e and S8), indicating the successful formation of a heterostructure catalyst.

The molar ratio of 2D $CoSe_2/Ni_{0.85}Se$ was obtained using inductively coupled plasma atomic emission spectroscopy (ICP-AES) and EDS measurements, as depicted in Fig. S3 and Table S1. The atomic ratio of Co/Ni/Se in the $CoSe_2/Ni_{0.85}Se$ measured by ICP is around 1:1.31:2.32, suggesting that the calculated molar ratio of $CoSe_2/Ni_{0.85}Se$ is around 1:1.16, as displayed in Table S1. Additionally, the molar ratio of $CoSe_2/Ni_{0.85}Se$ determined by EDS is around 1:1.19, in agreement with the ratio obtained from ICP analysis. Overall, the findings based on the structural and morphological characterizations proved that Co^{2+} and Ni^{2+} dual cations successfully integrated in the form of metal selenides as 2D $CoSe_2/Ni_{0.85}Se$ heterostructure.

X-ray photoelectron spectroscopy was applied to assess the surface chemical states and electron distribution between Co and Ni of 2D $CoSe_2/Ni_{0.85}Se$. The full XPS survey spectrum (Fig. S9) attests to the existence of Co, Ni, and Se in 2D $CoSe_2/Ni_{0.85}Se$. Two peaks were revealed by the XPS of Ni 2p in 2D $CoSe_2/Ni_{0.85}Se$ (Fig. 2b) at binding energies of 872.8 and 854.9 eV. These peaks are credited to Ni^{2+} $2p_{1/2}$ and $2p_{3/2}$, respectively [39]. This peak moved to high binding energy in comparison to $Ni_{0.85}Se$, indicating that electrons are transferred from Co
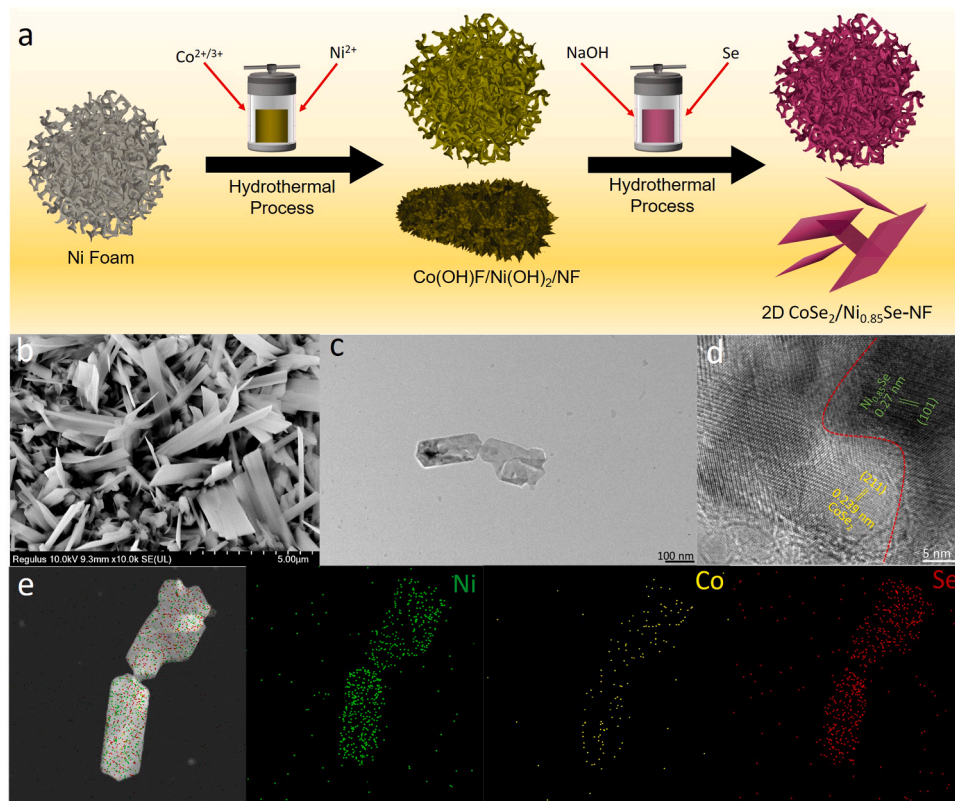

Fig. 1. (a) schematic diagram of the synthesis procedure for 2D $CoSe_2/Ni_{0.85}Se$ via hydrothermal method, (b) SEM image of 2D $CoSe_2/Ni_{0.85}Se$, (c) High magnification TEM image of 2D $CoSe_2/Ni_{0.85}Se$, (d) HRTEM image of 2D $CoSe_2/Ni_{0.85}Se$, (e) EDS mapping of 2D $CoSe_2/Ni_{0.85}Se$ showing the various elements.
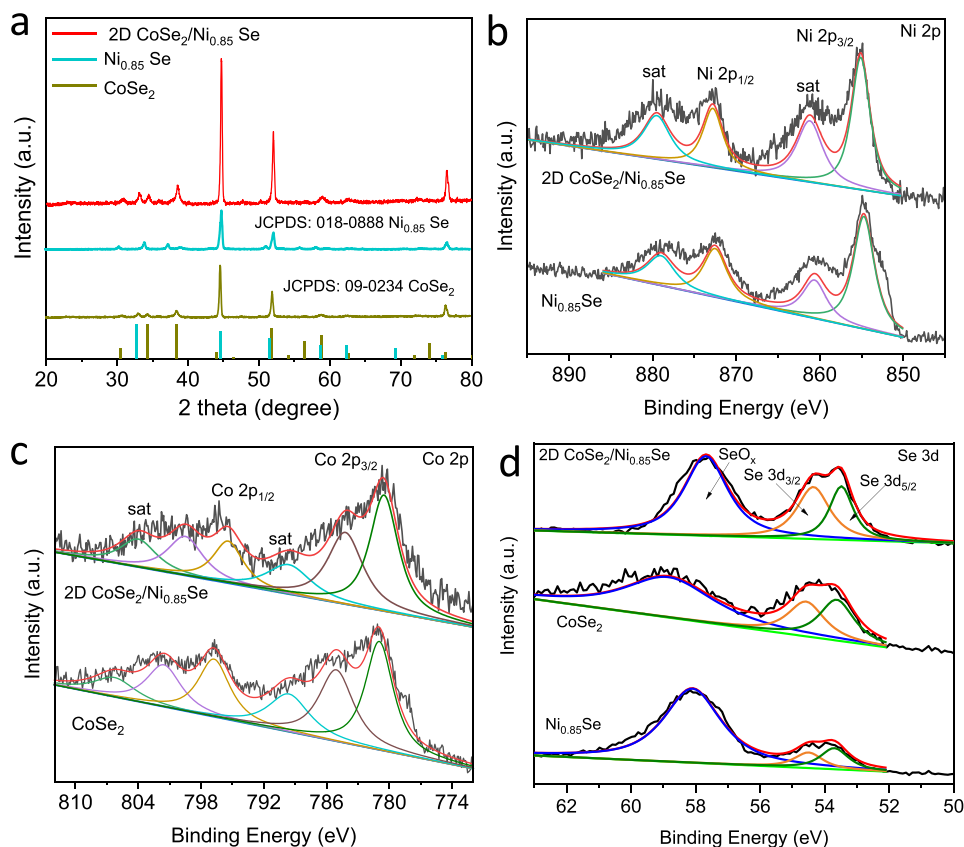
Fig. 2. (a) XRD pattern of 2D $CoSe_2/Ni_{0.85}Se$, $CoSe_2$ and $Ni_{0.85}Se$, High resolution XPS spectra (b) Ni 2p, (c) Co 2p and (d) Se 3d spectra of 2D $CoSe_2/Ni_{0.85}Se$.

to Ni atoms. Note that the other two signals belonging to Ni satellite peaks are also exhibited. This illustrates the optimized electronic structure of Ni sites as the electrons of Co are transferred to Ni due to the electronegativity difference between Ni (1.91) and Co (1.88). Furthermore, the high-resolution Co 2p XPS demonstrated binding energies of 780.2 and 796.4 eV, corresponding to Co^{2+} $2p_{3/2}$ and $2p_{1/2}$ in 2D $CoSe_2/Ni_{0.85}Se$. These peaks shifted to a low binding energy in comparison to $CoSe_2$ [40], as displayed in Fig. 2c. After the formation of the heterointerface, the XPS peak positions of Ni 2p and Co 2p differ noticeably (Table S2-S3), further supporting the strong transfer of electrons between catalysts. The two XPS peaks at 53.5 and 54.3 eV are linked with Se $3d_{5/2}$ and Se $3d_{3/2}$ in 2D $CoSe_2/Ni_{0.85}Se$, respectively, which also shifted to a lower binding energy when compared with $CoSe_2$ and $Ni_{0.85}Se$ (Fig. 2d). Note that the peak at 57.7 eV corresponding to Se-O species is observed as a result of surface oxidation [41]. Hence, the combined study shows that the hierarchical transition bimetal selenides heterostructure was successfully synthesized.

3.2. Electrochemical evaluation of UOR

The electrocatalytic performance of designed samples for UOR was investigated in 1.0 M KOH with 0.5 M urea solution in a standard three-electrode cell. Unless stated otherwise, all the potentials described here are reported versus reversible hydrogen electrodes (vs RHE). As shown in Fig. 3a, 2D $CoSe_2/Ni_{0.85}Se$ exhibited lower onset potential in the presence of 1.0 M KOH with 0.5 M urea compared to that in 1.0 M KOH. The potential needed for UOR to attain the current density of 100 mA cm^{-2} is about 1.33 V (vs RHE). The increased activity of 2D $CoSe_2/Ni_{0.85}Se$ for UOR was shown by the significant reduction in voltage of 90 mV expected to achieve the same current density of 100 mA cm^{-2} in comparison to OER performance in 1.0 M KOH. Next, the UOR activity of Co(OH)F/Ni(OH)$_2$, $CoSe_2$, $Ni_{0.85}Se$, and commercial

RuO_2 was also assessed in 1 M KOH + 0.5 M urea (Fig. 3b), and a relatively higher potential of 1.64, 1.59, 1.45, and 1.72 V, respectively, is achieved as compared with the 2D $CoSe_2/Ni_{0.85}Se$ (1.33 V). It is also interesting to see that the 2D $CoSe_2/Ni_{0.85}Se$ nanoplate showed the lowest potentials of 1.33 and 1.43 V to attain 100 and 200 mA cm^{-2}, as shown in Fig. 3c.

The resulting Tafel slopes derived from steady-state polarization curves for all samples were calculated and displayed in Fig. 3d and S10 to reveal the UOR kinetics. The Tafel slope analysis was verified using chronoamperometry measurements, which eliminate capacitive current and improve accuracy [42]. Considerably, 2D $CoSe_2/Ni_{0.85}Se$ revealed a Tafel slope of 26 mV dec^{-1}, which is lower when compared with $CoSe_2$ (36.7 mV dec^{-1}), $Ni_{0.85}Se$ (32.4 mV dec^{-1}), Co(OH)F/Ni(OH)$_2$ (52.5 mV dec^{-1}) and RuO_2 (73.2 mV dec^{-1}), indicating higher activity and increased kinetics for UOR. The superior performance of 2D $CoSe_2/Ni_{0.85}Se$ for UOR also surpasses most of the recently reported works, as displayed in Fig. 3e and Table S4. The double-layer capacitance (C_{dl}), which is correlated with the electrochemical active surface area (ECSA), was analyzed using the CV test at various scan speeds at the non-faradaic region to ascertain the reasons for a comparatively higher UOR activity of 2D $CoSe_2/Ni_{0.85}Se$ (Fig. S11). As shown in Fig. 3f, the calculated C_{dl} values for the catalysts 2D $CoSe_2/Ni_{0.85}Se$ (4.62 mF cm^{-2}) are higher than Co(OH)F/Ni(OH)$_2$ (1.44 mF cm^{-2}), $Ni_{0.85}Se$ (2.96 mF cm^{-2}), and $CoSe_2$ (2.46 mF cm^{-2}), indicating 2D $CoSe_2/Ni_{0.85}Se$ has higher ECSA and the most exposed active sites in UOR. Moreover, as displayed in Fig. S12, the specific activity of the designed catalysts was analyzed by normalizing the current density with ECSA to determine the catalyst's intrinsic activity.

The turnover frequency (TOF) values for 2D $CoSe_2/Ni_{0.85}Se$, $CoSe_2$, and $Ni_{0.85}Se$ were analyzed and compared using an electrochemical approach (Fig. S13). The TOF for 2D $CoSe_2/Ni_{0.85}Se$ (0.753 s^{-1} at 1.4 V) is higher than that for $CoSe_2$ (0.53 s^{-1}) and $Ni_{0.85}Se$ (0.637 s^{-1}). From
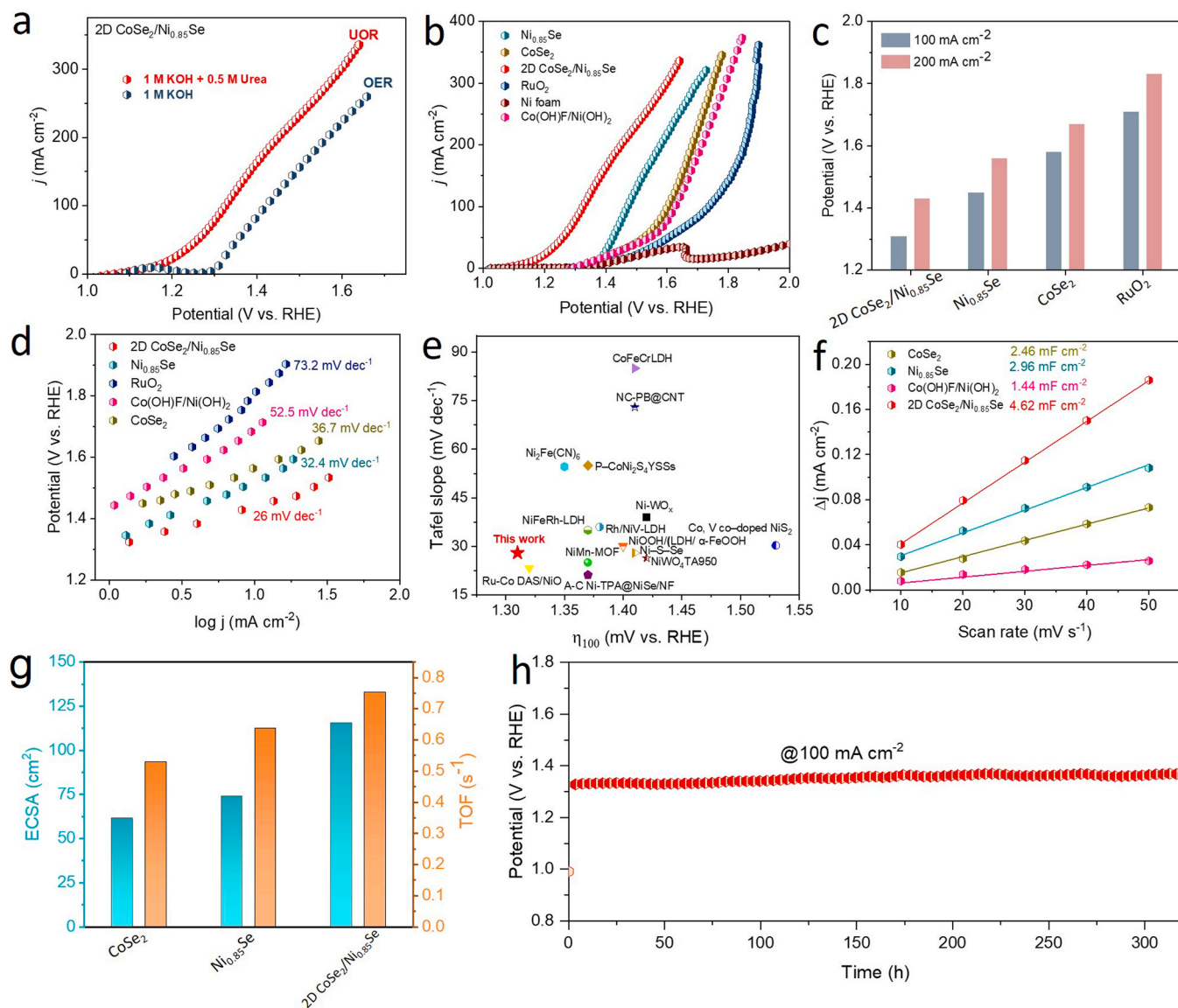
Fig. 3. Evaluation of the UOR electrocatalytic performance. (a) LSV curves of 2D $CoSe_2/Ni_{0.85}Se$ electrocatalysts in 1.0 M KOH with and without 0.5 M urea, (b) Polarization curves of NF, $Co(OH)F/Ni(OH)_2$, $Ni_{0.85}Se$, $CoSe_2$, and 2D $CoSe_2/Ni_{0.85}Se$, (c) Comparison of potentials at 100 and 200 mA cm^{-2} current densities, (d) Tafel plots, (e) Comparison of the overpotential of 2D $CoSe_2/Ni_{0.85}Se$ at a current density of 100 mA cm^{-2} with other reported works, (f) Plots of current density against scan rates of $Co(OH)F/Ni(OH)_2$, $Ni_{0.85}Se$, $CoSe_2$, and 2D $CoSe_2/Ni_{0.85}Se$ in 1 M KOH with 0.5 M urea, (g) ECSA and TOFs of the different catalysts, (h) Chronopotentiometry test of 2D $CoSe_2/Ni_{0.85}Se$ at a current density of 100 mA cm^{-2}.

Fig. 3g, the ECSA and TOF of 2D $CoSe_2/Ni_{0.85}Se$ are superior to $CoSe_2$ and $Ni_{0.85}Se$, suggesting that the formation of heterointerface with two active sites (Co^{2+}/Ni^{2+}) in 2D $CoSe_2/Ni_{0.85}Se$ is the major contributor to high intrinsic activity for UOR. Moreover, long-term stability is another significant factor to take into account when assessing the performance of a catalyst for UOR. As can be noted from Fig. S14, no change is seen in the catalytic activity of 2D $CoSe_2/Ni_{0.85}Se$ after 2000 CV cycles, suggesting strong durability of the as-synthesized electrode for UOR. The long-term stability of 2D $CoSe_2/Ni_{0.85}Se$ was further examined via chronopotentiometry, and slight deactivation was seen at 100 mA cm^{-2} during continuous operation for more than 300 h, highlighting the catalyst potential for UOR-related processes (Fig. 3h). The gas generated from 2D $CoSe_2/Ni_{0.85}Se$ electrode was bubbled into a transparent Ca $(OH)_2$ solution using argon gas. The transparent $Ca(OH)_2$ solution exhibited turbidity, indicating the presence of CO_2 gas in the product resulting from the UOR process (Fig. S15). Quantification of urea after the stability test is displayed in Fig S16.

Post-UOR characterization was also investigated to uncover more

about the morphology and chemical composition of 2D $CoSe_2/Ni_{0.85}Se$. As seen in Fig. S17-19, XRD, SEM, and EDS mapping showed strong structural stability of 2D $CoSe_2/Ni_{0.85}Se$, demonstrated by the well-preserved nanoplate morphology and crystal structure. Moreover, XPS spectra of the post-UOR samples were carried out to explore the chemical state of 2D $CoSe_2/Ni_{0.85}Se$, as displayed in Fig. S20. The XPS spectrum of Ni 2p in 2D $CoSe_2/Ni_{0.85}Se$ after UOR shifted to a lower binding energy when compared with the fresh 2D $CoSe_2/Ni_{0.85}Se$ sample and showed two distinct peaks at 854.19 and 872 eV which is ascribed to Ni^{3+} in $Ni_{0.85}Se$ [43]. The XPS spectra of Co 2p in 2D $CoSe_2/Ni_{0.85}Se$ slightly shifted to higher binding energy after the UOR stability test when compared with 2D $CoSe_2/Ni_{0.85}Se$ [44].

Quasi-in situ electrochemical impedance spectroscopy (EIS) is a useful characterization method for monitoring the activity of the catalysts' evolving surface kinetics, electron, and mass transfer during the catalytic reaction [45]. To unravel the electrochemical UOR mechanism, Quasi-in situ EIS test was conducted in 1 M KOH with 0.5 M urea utilizing the as-synthesized electrocatalysts 2D $CoSe_2/Ni_{0.85}Se$, $CoSe_2$, and

$Ni_{0.85}Se$. According to Fig. 4a, the 2D $CoSe_2/Ni_{0.85}Se$ (5.9 Ω) has significantly lower charge resistance (R_{ct}) than $Ni_{0.85}Se$ (10.4 Ω), $CoSe_2$ (16.7 Ω), and $Co(OH)F/Ni(OH)_2$ (28.2 Ω), signifying rapid reaction kinetics for 2D $CoSe_2/Ni_{0.85}Se$.

The potential dependent EIS test in Fig. 4b-d further depicts measured impedance at different voltages for R_{ct} and the reaction kinetics during the UOR process. The measured impedance of 2D $CoSe_2/Ni_{0.85}Se$ exhibited the lowest R_{ct} when compared to $CoSe_2$ and $Ni_{0.85}Se$, which confirms that the formation of heterostructure catalyst enhances the R_{ct} and adsorption of intermediates during the UOR process [46,47]. To determine the significant fitting parameters R_{ct}, the Nyquist plots should be fitted by similar circuit diagrams. When compared to $CoSe_2$ and $Ni_{0.85}Se$, the fitting changes for R_{ct} (Fig. 4e) demonstrate that 2D $CoSe_2/Ni_{0.85}Se$ R_{ct} is lower, suggesting that the UOR activity exhibits rapid reaction kinetics, as shown in Table S5-7. The Bode phase plots also display the phase angle as a function of frequency at various potentials, as seen in Fig. 4f-h. According to the Bode phase plots, the phase angle of the low-frequency areas of the three catalysts considerably reduced during the UOR process [3,13]. Additionally, the phase angle of the low-frequency region for $CoSe_2$ (Fig. 4f) and $Ni_{0.85}Se$ (Fig. 4g) catalysts exceeded 1.35 and 1.40 V vs. RHE, respectively, indicating passivation reaction caused by the competition between UOR and OER [13,48]. Furthermore, the diameter of the low-frequency phase angle of 2D $CoSe_2/Ni_{0.85}Se$ heterointerface catalyst reduces throughout the whole potential window, indicating high UOR selectivity of 2D $CoSe_2/Ni_{0.85}Se$ (Fig. 4h). The lower phase peak angle of 2D $CoSe_2/Ni_{0.85}Se$ as displayed in Fig. 4i in the low-frequency region suggests that the formation of heterointerface is vital for rapid UOR kinetics.

3.3. Urea-assisted anion-exchange membrane electrolyzer

Considering the superior activity of 2D $CoSe_2/Ni_{0.85}Se$ for UOR, we designed an electrolyzer for urea electrolysis with 2D $CoSe_2/Ni_{0.85}Se$ as the anode and com Pt/C as the cathode. As displayed in Fig. S21, the 2D $CoSe_2/Ni_{0.85}Se$ heterostructure catalyst exhibited superior performance when compared to RuO_2 at 100 mA cm^{-2}. Furthermore, we constructed a urea-assisted anion exchange membrane (AEM) electrolyzer (Fig. 5a and S22, Supporting Information). This electrolyzer was built using 2D
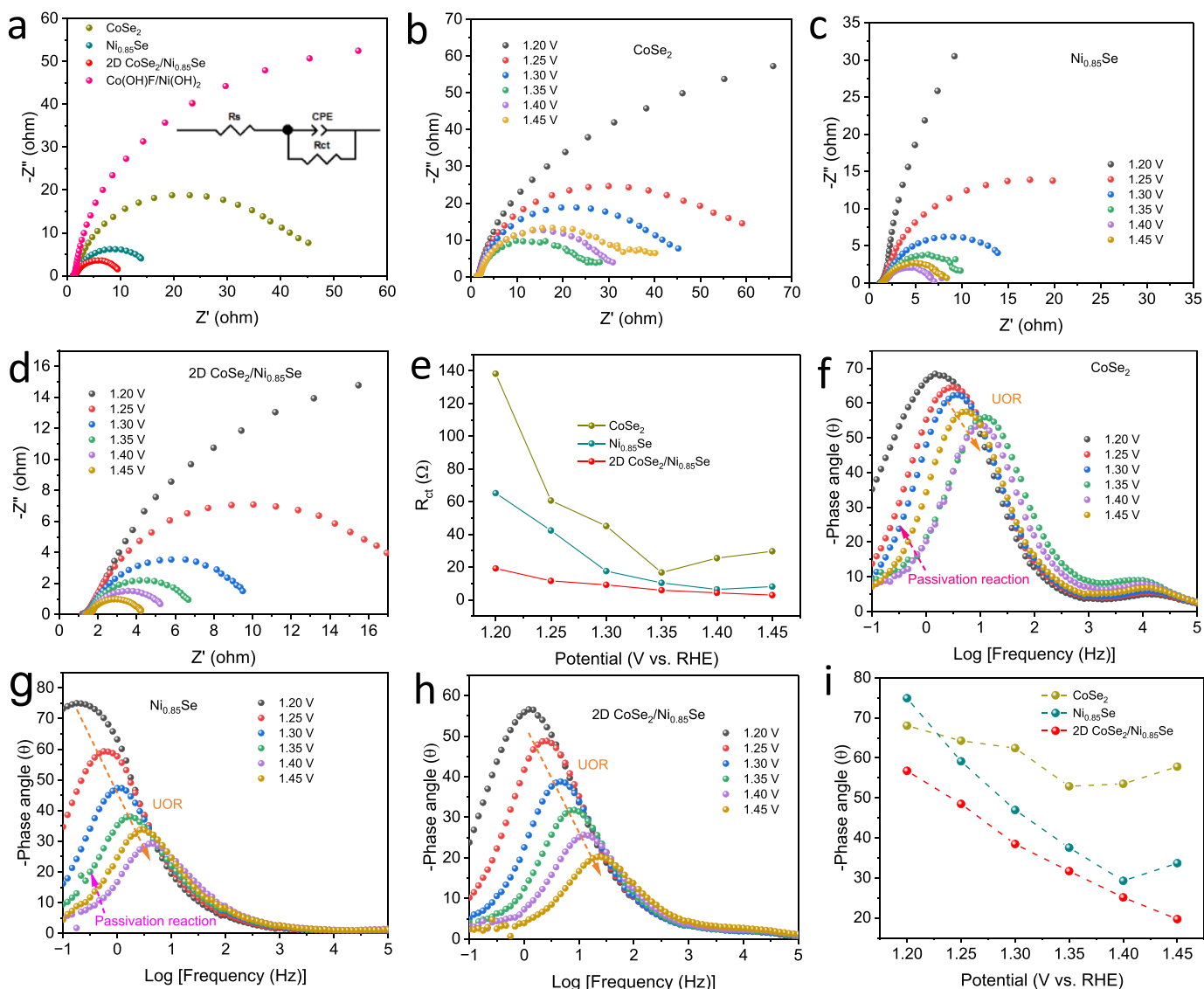

Fig. 4. Quasi-In Situ EIS. (a) Nyquist plots for $Co(OH)F/Ni(OH)_2$, $Ni_{0.85}Se$, $CoSe_2$, and 2D $CoSe_2/Ni_{0.85}Se$ at 1.35 V vs. RHE, Nyquist plots of (b) $CoSe_2$, (c) $Ni_{0.85}Se$, and (d) 2D $CoSe_2/Ni_{0.85}Se$ at different applied potentials (1.2–1.45 V vs. RHE) in 1 M KOH electrolyte containing 0.5 M urea, (e) Response of the charge transfer resistance (R_{ct}) at different potentials for $Ni_{0.85}Se$, $CoSe_2$, and 2D $CoSe_2/Ni_{0.85}Se$ electrodes, Bode phase plots for (f) $CoSe_2$, (g) $Ni_{0.85}Se$, (h), and 2D $CoSe_2/Ni_{0.85}Se$ at different potentials (1.2–1.45 V vs. RHE), (i) Comparison of phase peak angles of $Ni_{0.85}Se$, $CoSe_2$ and 2D $CoSe_2/Ni_{0.85}Se$ at different potentials.
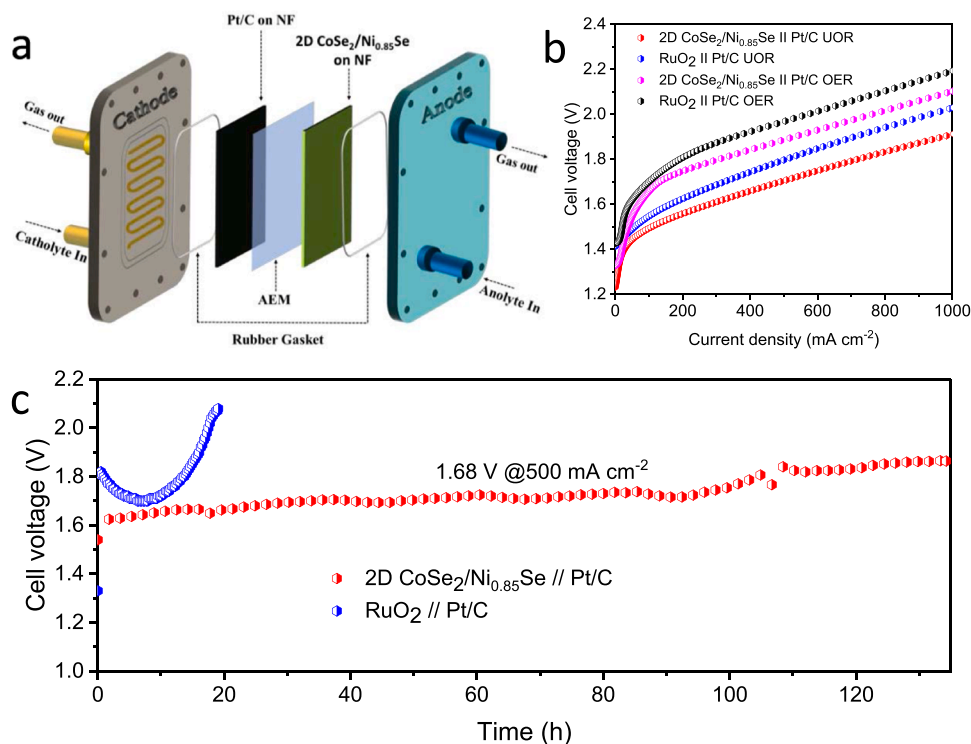
Fig. 5. OER replacement by the UOR in urea-assisted AEM electrolyzer for hydrogen production. (a) Schematic of the urea-assisted AEM electrolyzer, (b) Comparison of LSV for UOR//HER and OER//HER using 2D $CoSe_2/Ni_{0.85}Se$ electrode as anode, (c) Stability of the urea-assisted AEM electrolyzer at 500 mA cm^{-2} for 120 h at 50 °C in 1 M KOH with 0.5 M urea.

$CoSe_2/Ni_{0.85}Se$ as the anodic and Pt/C as the cathodic electrode, respectively. The polarization curves for 2D $CoSe_2/Ni_{0.85}Se$ and RuO_2 in 1 M KOH with and without 0.5 M urea are shown in Fig. 5b. As anticipated, at a cell potential of 1.73 V, the 2D $CoSe_2/Ni_{0.85}Se$ catalyst achieved a UOR current density of 600 mA cm^{-2}, which is greater than the RuO_2 catalyst (400 mA cm^{-2}). The urea-assisted AEM electrolyzer also showed strong durability for 2D $CoSe_2/Ni_{0.85}Se$ catalysts. The urea-assisted electrolyzer generated 500 mA cm^{-2} at 1.68 V for 120 h with no discernible rise in voltage, demonstrating the possibility of large-scale energy-saving H_2 generation as illustrated in Fig. 5c. Additionally, this electrolyzer is capable of realizing an industrial current density of 1 A cm^{-2} to attain a voltage of 1.91 V, which is superior to $RuO_2||Pt/C$ under the same conditions and operates steadily for more than 20 h with a slight degradation as exhibited in Fig. S23.

3.4. Mechanism of electrocatalytic urea oxidation reaction

Experimental efforts unveiled that the rationally synthesized 2D $CoSe_2/Ni_{0.85}Se$ showed superior catalytic activity and robust stability. To further understand the reaction mechanism and the underlying reason for the higher activity, in-situ infrared reflection-absorption spectroscopy (IRRAS) and density functional theory (DFT) simulations were conducted. From the in situ IRRAS result in Fig. 6a, the C-N stretching vibration peak for urea adsorbate on 2D $CoSe_2/Ni_{0.85}Se$ is observed at 1410 cm^{-1}, and its intensity rises with applied voltage [49]. Additionally, the 2D $CoSe_2/Ni_{0.85}Se$ catalyst spectra showed a peak at 1701 cm^{-1} which is attributed to the C$=$O vibration intermediate [40]. As the potential is increased, it is found that the CO_2 vibration peaks at 2390 cm^{-1} increased in 2D $CoSe_2/Ni_{0.85}Se$ [50], which is in direct opposition to $Ni_{0.85}Se$ and $CoSe_2$ (Fig. S24) minimal change in CO_2 vibration peaks and indicates rapid reaction kinetics of CO_2 desorption in 2D $CoSe_2/Ni_{0.85}Se$. The urea molecule first undertakes a dehydrogenation process to generate $CO(NH_2)_2*$ on 2D $CoSe_2/Ni_{0.85}Se$, $CoSe_2$, and $Ni_{0.85}Se$ which corresponds to an energy of −0.42, −0.35, and −0.38 eV,

respectively (Fig. 6f).

As observed in Fig. 6a, the N–H vibration in amide (-NH) groups, which is thought to be the key intermediate during urea oxidation, was responsible for the peak discovered at 2950 cm^{-1} [29]. In comparison with the $CoSe_2$ and $Ni_{0.85}Se$ counterparts, the 2D $CoSe_2/Ni_{0.85}Se$ enhanced C-N fragmentation facilitates *NH adsorption, resulting in a high *NH adsorption and less OH- coverage, thus inhibiting OER during UOR. As a result, the UOR energetics for the C–N fragmentation route with various local concentrations of urea adsorbate on 2D $CoSe_2/Ni_{0.85}Se$ were observed. Further, DFT calculations were conducted to investigate the distinct UOR reaction pathway on prepared 2D $CoSe_2/Ni_{0.85}Se$ heterointerface in more detail. The 2D $CoSe_2/Ni_{0.85}Se$ atomic structure model was designed based on findings corroborated by experimental characterizations, where dual metal cations species $Co^{2+/3+}/Ni^{2+}$ are more dominant in the vicinity close to the surface and Se atoms are mostly located on the surface sections (Fig. S25).

To further analyze the electronic structure of the catalyst, the projected density of states (PDOS) and partial DOS for 2D $CoSe_2/Ni_{0.85}Se$, $Ni_{0.85}Se$, and $CoSe_2$ (Fig. 6b and Fig. S26-29) was computed. The results indicated much distribution of density of states over the Fermi level for the 2D $CoSe_2/Ni_{0.85}Se$ heterointerface as compared to $CoSe_2$, and $Ni_{0.85}Se$ species. Moreover, PDOS studies of 2D $CoSe_2/Ni_{0.85}Se$ heterointerface (Fig. 6b) suggested high involvement of the d-orbital of both transition metals in the density of states. This finding implies a significant improvement in electrical conductivity and electron transport in 2D $CoSe_2/Ni_{0.85}Se$, which is advantageous for boosting electron transfer during UOR for enhanced activity. Hence, 2D $CoSe_2/Ni_{0.85}Se$ can boost the charge transfer for UOR which could be credited to the heterointerface formed. Fig. 6c depicts the primary UOR reaction pathway on the 2D $CoSe_2/Ni_{0.85}Se$ heterointerface catalyst. The Co element within the heterostructure catalyst was primarily employed to increase the activity of the $Ni_{0.85}Se$ catalyst due to an appropriate electronic configuration Co-atom, which might promote electronic communication at the $CoSe_2/Ni_{0.85}Se$ materials heterointerface.
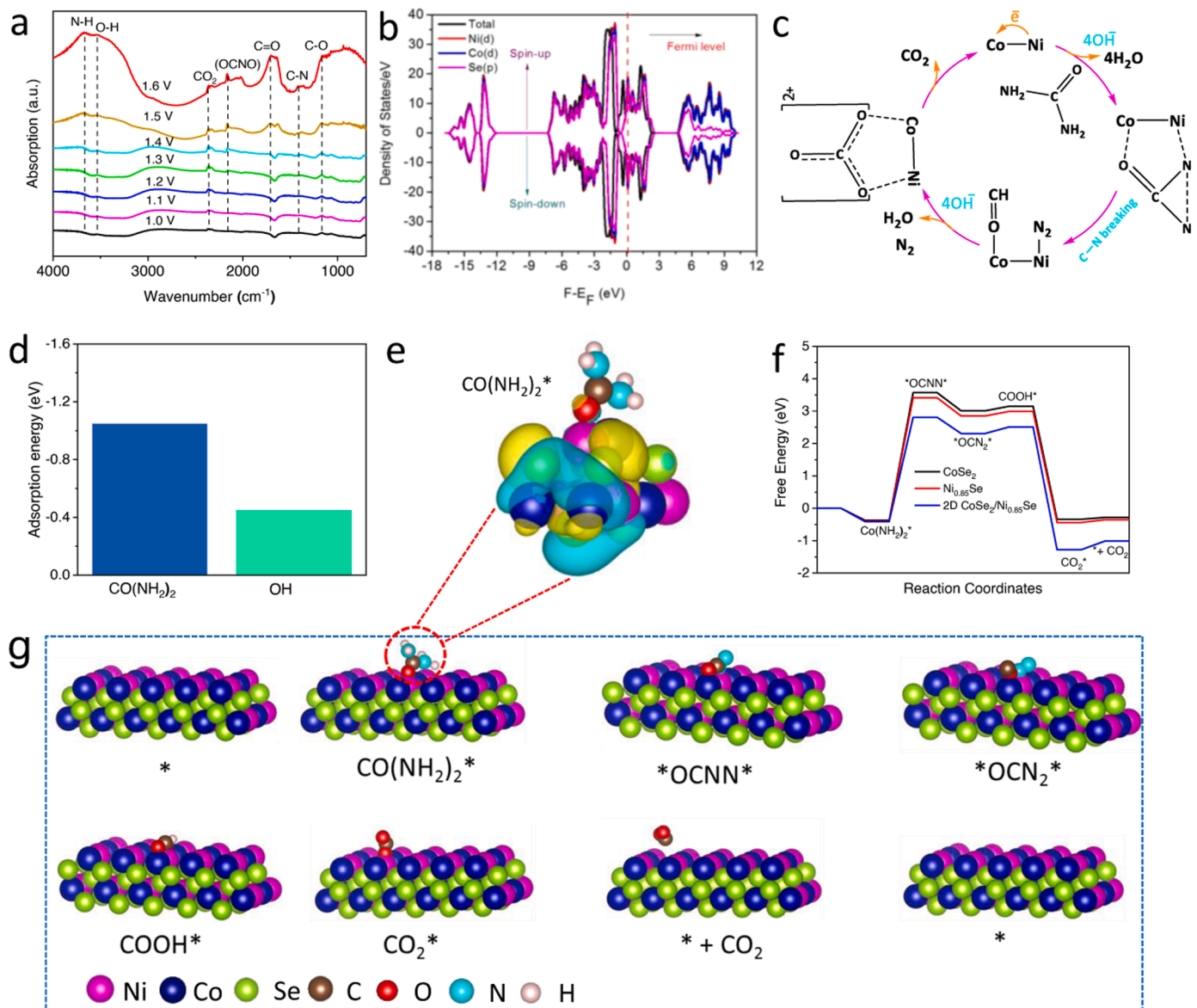
Fig. 6. Insight into catalytic activity and reaction mechanism. (a) In situ IRRAS for 2D $CoSe_2$/$Ni_{0.85}$Se in the range of 700–4000 cm^{-1} at different potentials during the UOR process, (b) PDOS of Ni(d), Co(d), and Se(p) orbitals in the 2D $CoSe_2$/$Ni_{0.85}$Se, (c) Possible UOR mechanism on the 2D $CoSe_2$/$Ni_{0.85}$Se electrode, (d) Adsorption energy of $CO(NH_2)_2$* and OH*, (e) Charge density difference for 2D $CoSe_2$/$Ni_{0.85}$Se, (f) Free energy diagram of the UOR on 2D $CoSe_2$/$Ni_{0.85}$Se, (g) Schematic illustration of the proposed UOR mechanisms.

Moreover, the formation of a heterointerface between $CoSe_2$ and $Ni_{0.85}$Se material offered a dual-atomic arrangement in appropriate proximity to catalyze the urea electrooxidation. In the initial stage, the catalyst surface facilitated the adsorption of urea molecules. Subsequently, the removal of four hydrogen atoms resulted in the formation of an intermediate species (*CON_2). The Co- and Ni- atoms of this intermediate species then underwent coupling with O- and N-atoms, respectively, because of the high affinity of O-atom towards the Co-element. It is important to note that the strong C–N bond must be immediately broken with the evacuated energy of 1.89 eV. Nonetheless, if the intermolecular N–N coupling mechanism is linked, C–N breaking will be very simple since the energy produced during N–N coupling will be equivalent to the energy needed for C–N cleavage. Based on published studies, we conjectured that N–N coupling preceded the breakage of the C–N bond [29,51]. When the potential is applied, the two N atoms on the CON_2 intermediate separate to produce N_2 and discharge Ni active sites. Concurrently, the residue of C═O was penetrated by OH$^-$ to generate the OH–C═O structure.

The adsorption behavior of intermediates and reaction mechanism on the 2D $CoSe_2$/$Ni_{0.85}$Se heterostructure is further investigated after analyzing its intrinsic electronic characteristics. Initially, the competitive adsorption behavior between $CO(NH_2)_2$* and OH* on 2D $CoSe_2$/$Ni_{0.85}$Se was investigated. Urea may be able to fill the Ni active sites more efficiently than OH*, as displayed in Fig. 6d, where the adsorption energy of $CO(NH_2)_2$ on 2D $CoSe_2$/$Ni_{0.85}$Se is −1.05 eV, which is considerably lower than the adsorption of OH (-0.45 eV). This creates the likelihood of UOR occurring before OER since UOR requires the adsorption of urea molecules. According to the charge density difference of 2D $CoSe_2$/$Ni_{0.85}$Se-$CO(NH_2)_2$ adduct, there are significant electron transfers at the heterointerface between $Ni_{0.85}$Se and $CoSe_2$, as well linker site (O*) of urea, indicating the charge redistribution and electronic interaction within the 2D $CoSe_2$/$Ni_{0.85}$Se heterointerface, as well as urea adsorption on Co site, as shown in Fig. 6e. The calculated free energy diagram for 2D $CoSe_2$/$Ni_{0.85}$Se heterointerface showed a lower Gibbs free energy when compared to $Ni_{0.85}$Se and $CoSe_2$, as shown in Fig. 6f and Table S8. Thus, theoretical simulations show the

thermodynamically favorable process of UOR on the surface of a 2D $CoSe_2/Ni_{0.85}Se$ heterointerface catalyst supporting the viability of triggering UOR via the heterostructure engineering technique. This suggests that the 2D $CoSe_2/Ni_{0.85}Se$ heterointerface catalyst is preferable for the desorption of CO_2 than the $Ni_{0.85}Se$ and $CoSe_2$, which is consistent with the observation of CO_2 release by the In-situ IRRAS analysis. Hence, the suggested UOR mechanism on the 2D $CoSe_2/Ni_{0.85}Se$ surface is CO $(NH_2)_2^* \to {}^*OCNN^* \to {}^*OCN_2^* \to COOH^* \to CO_2^* \to {}^*+CO_2$ as seen in Fig. 6g.

4. Conclusion

In summary, the 2D $CoSe_2/Ni_{0.85}Se$ nanoplate heterostructure was fabricated through a feasible two-step hydrothermal treatment as an efficient and stable electrocatalyst for UOR. Benefiting from heterostructure engineering with synergistic effects within 2D $CoSe_2/Ni_{0.85}Se$, the electrocatalyst exhibited UOR performance at a very low potential of 1.33 V at 100 mA cm^{-2}, as well as impressive strong durability with no noticeable deterioration for more than 300 h of operation. Additionally, using 2D $CoSe_2/Ni_{0.85}Se$ as the anode for a single-cell AEM urea electrolyzer enables this electrode to attain an industrial current density of 1 A cm^{-2} at a voltage of 1.91 V while maintaining strong durability. Density functional theory simulations indicate that the interface interaction between $CoSe_2$ and $Ni_{0.85}Se$ enhances adsorption energies and UOR kinetics, hence improving the electrocatalytic activity. This study offers new perspectives on the development of efficient heterostructure catalysts for potential applications in the electrosynthesis of chemicals/ fuels as well as green energy conversion and storage.

CRediT authorship contribution statement

Felix Ofori Boakye: Conceptualization, Resources, Methodology, Visualization, Formal analysis, Investigation, Data curation, Writing-original draft, Writing-review & editing. **Marshet Getaye Sendeku:** Conceptualization, Data curation, Supervision, Writing-review & editing. **Anuj Kumar:** Conceptualization, DFT calculation. **Saira Ajmal:** Formal analysis, Validation. **Kwadwo Asare Owusu:** Resources, Validation, Methodology. **Kassa Belay Ibrahim:** Resources, Validation, Methodology. **Mohammad Tabish:** Resources, Validation, Methodology. **Fakhr uz Zaman:** Data curation, Validation. **Muhammad Asim Mushtaq:** Methodology, Visualization. **Khalid M. Alotaibi:** Validation, Methodology. **Mohd Zahid Ansari:** Formal Analysis, Visualization. **Ghulam Yasin:** Conceptualization, Project administration, Supervision, Writing-review & editing, Funding acquisition.

Declaration of Competing Interest

The authors declare that they have no known competing financial interests or personal relationships that could have appeared to influence the work reported in this paper.

Data availability

Data will be made available on request.

Acknowledgements

Appendix A. Supporting information

Supplementary data associated with this article can be found in the online version at doi:10.1016/j.apcatb.2024.124013.

References

[1] Y. Zhu, C. Liu, S. Cui, Z. Lu, J. Ye, Y. Wen, W. Shi, X. Huang, L. Xue, J. Bian, Multistep dissolution of lamellar crystals generates superthin amorphous Ni (OH) 2 catalyst for UOR, Adv. Mater. (2023) 2301549.

[2] Y. Zhou, Y. Wang, D. Kong, Q. Zhao, L. Zhao, J. Zhang, X. Chen, Y. Li, Y. Xu, C. Meng, Revealing the reactant mediation role of low-valence Mo for accelerated urea-assisted water splitting, Adv. Funct. Mater. 33 (2023) 2210656.

[3] Y. Feng, N. Ran, X. Wang, Q. Liu, J. Wang, L. Liu, K. Suenaga, W. Zhong, R. Ma, J. Liu, Nanoparticulate WN/Ni$_3$C coupling in ceramic coatings for boosted urea electro-oxidation, Adv. Energy Mater. (2023) 2302452.

[4] M. Cai, Q. Zhu, X. Wang, Z. Shao, L. Yao, H. Zeng, X. Wu, J. Chen, K. Huang, S. Feng, Formation and stabilization of NiOOH by introducing α-FeOOH in LDH: composite electrocatalyst for oxygen evolution and urea oxidation reactions, Adv. Mater. 35 (2023) 2209338.

[5] C. Bozal-Ginesta, R.R. Rao, C.A. Mesa, Y. Wang, Y. Zhao, G. Hu, D. Antón-García, I. E. Stephens, E. Reisner, G.W. Brudvig, Spectroelectrochemistry of water oxidation kinetics in molecular versus heterogeneous oxide iridium electrocatalysts, J. Am. Chem. Soc. 144 (2022) 8454–8459.

[6] X. Zheng, J. Yang, P. Li, Z. Jiang, P. Zhu, Q. Wang, J. Wu, E. Zhang, W. Sun, S. Dou, Dual-atom support boosts nickel-catalyzed urea electrooxidation, Angew. Chem. Int. Ed. 62 (2023) e202217449.

[7] C. Wang, Q. Wang, X. Du, X. Zhang, Controlled synthesis of M doped NiVS (M= Co, Ce and Cr) as a robust electrocatalyst for urea electrolysis, Dalton Trans. 52 (2023) 13161–13168.

[8] X.F. Lu, S.L. Zhang, W.L. Sim, S. Gao, X.W. Lou, Phosphorized CoNi$_2$S$_4$ yolk-shell spheres for highly efficient hydrogen production via water and urea electrolysis, Angew. Chem. 133 (2021) 23067–23073.

[9] T. Yu, Q. Xu, J. Chen, G. Qian, X. Zhuo, H. Yang, S. Yin, Boosting urea-assisted water splitting by constructing sphere-flower-like NiSe$_2$-NiMoO$_4$ heterostructure, Chem. Eng. J. 449 (2022) 137791.

[10] P. Li, Y. Wang, X. Du, X. Zhang, Controlled synthesis of ACo $_2$ O $_4$ (A= Fe, Cu, Zn, Ni) as an environmentally friendly electrocatalyst for urea electrolysis, Dalton Trans. 52 (2023) 10499–10506.

[11] Y. Cao, T. Wang, X. Li, L. Zhang, Y. Luo, F. Zhang, A.M. Asiri, J. Hu, Q. Liu, X. Sun, A hierarchical CuO@ NiCo layered double hydroxide core–shell nanoarray as an efficient electrocatalyst for the oxygen evolution reaction, Inorg. Chem. Front. 8 (2021) 3049–3054.

[12] R. Lin, L. Kang, T. Zhao, J. Feng, V. Celorrio, G. Zhang, G. Cibin, A. Kucernak, D. J. Brett, F. Cora, Identification and manipulation of dynamic active site deficiency-induced competing reactions in electrocatalytic oxidation processes, Energy Environ. Sci. 15 (2022) 2386–2396.

[13] Y. Liao, Y. Chen, L. Li, S. Luo, Y. Qing, C. Tian, H. Xu, J. Zhang, Y. Wu, Ultrafine homologous Ni$_2$P-Co$_2$P heterostructures via space-confined topological transformation for superior urea electrolysis, Adv. Funct. Mater. 33 (2023) 2303300.

[14] C. Wang, H. Lu, Z. Mao, C. Yan, G. Shen, X. Wang, Bimetal Schottky heterojunction boosting energy-saving hydrogen production from alkaline water via urea electrocatalysis, Adv. Funct. Mater. 30 (2020) 2000556.

[15] S.-K. Geng, Y. Zheng, S.-Q. Li, H. Su, X. Zhao, J. Hu, H.-B. Shu, M. Jaroniec, P. Chen, Q.-H. Liu, Nickel ferrocyanide as a high-performance urea oxidation electrocatalyst, Nat. Energy 6 (2021) 904–912.

[16] K. Ke, G. Wang, D. Cao, G. Wang, Recent advances in the electro-oxidation of urea for direct urea fuel cell and urea electrolysis, Electrocatal (2020) 41–78.

[17] L. Wang, Y. Zhu, Y. Wen, S. Li, C. Cui, F. Ni, Y. Liu, H. Lin, Y. Li, H. Peng, Regulating the local charge distribution of Ni active sites for the urea oxidation reaction, Angew. Chem. 133 (2021) 10671–10676.

[18] L. Qiao, A. Zhu, D. Liu, J. Feng, Y. Chen, M. Chen, P. Zhou, L. Yin, R. Wu, K.W. Ng, Crystalline phosphides/amorphous oxides composite for energy-saving hydrogen production assisted by efficient urea oxidation reaction, Chem. Eng. J. 454 (2023) 140380.

[19] M. Zhong, J. Yang, M. Xu, S. Ren, X. Chen, C. Wang, M. Gao, X. Lu, Significantly enhanced energy-saving H$_2$ production coupled with urea oxidation by low-and non-Pt anchored on NiS-based conductive nanofibers, Small (2023) 2304782.

[20] H. Xie, Y. Feng, X. He, Y. Zhu, Z. Li, H. Liu, S. Zeng, Q. Qian, G. Zhang, Construction of nitrogen-doped biphasic transition-metal sulfide nanosheet electrode for energy-efficient hydrogen production via urea electrolysis, Small 19 (2023) 2207425.

[21] X. Xu, X. Wei, L. Xu, M. Huang, A. Toghan, Elucidating the promotion mechanism of the ternary cooperative heterostructure toward industrial-level urea oxidation catalysis, J. Energy Chem. (2023).

[22] N. Chen, Y.-X. Du, G. Zhang, W.-T. Lu, F.-F. Cao, Amorphous nickel sulfoselenide for efficient electrochemical urea-assisted hydrogen production in alkaline media, Nano Energy 81 (2021) 105605.

[23] Y. Zhou, B. Chu, Z. Sun, L. Dong, F. Wang, B. Li, M. Fan, Z. Chen, Surface reconstruction and charge distribution enabling Ni/W$_5$N$_4$ Mott-Schottky heterojunction bifunctional electrocatalyst for efficient urea-assisted water electrolysis at a large current density, Appl. Catal. B: Environ. 323 (2023) 122168.

[24] T. Yue, T. Shi, Y. Ji, J. Jia, Y. Chang, J. Chen, M. Jia, Interfacial engineering of nickel selenide with CeO$_2$ on N-doped carbon nanosheets for efficient methanol and urea electro-oxidation, J. Colloid Interface Sci. 653 (2024) 1369–1378.

[25] P. Zhai, Y. Zhang, Y. Wu, J. Gao, B. Zhang, S. Cao, Y. Zhang, Z. Li, L. Sun, J. Hou, Engineering active sites on hierarchical transition bimetal oxides/sulfides

heterostructure array enabling robust overall water splitting, Nat. Commun. 11 (2020) 5462.

[26] X. Xu, J. Li, C. Zhang, S. Zhang, G. Su, Z. Shi, H. Wang, M. Huang, Controllable transition engineering from homogeneous $NiSe_2$ nanowrinkles to heterogeneous $Ni_3Se_4/NiSe_2$ rod-like nanoarrays for promoted urea-rich water oxidation at large current densities, Appl. Catal. B: Environ. 319 (2022) 121949.

[27] Z. Liu, C. Zhang, H. Liu, L. Feng, Efficient synergism of $NiSe_2$ nanoparticle/NiO nanosheet for energy-relevant water and urea electrocatalysis, Appl. Catal. B: Environ. 276 (2020) 119165.

[28] X. Xu, H. Liao, L. Huang, S. Chen, R. Wang, S. Wu, Y. Wu, Z. Sun, H. Huang, Surface reconstruction and directed electron transport in $NiSe_2/MoSe_2$ Mott-Schottky heterojunction catalysts promote urea-assisted water splitting, Appl. Catal. B: Environ. 341 (2024) 123312.

[29] L. Jin, R. Ji, H. Wan, J. He, P. Gu, H. Lin, Q. Xu, J. Lu, Boosting the electrocatalytic urea oxidation performance by amorphous–crystalline Ni-TPA@ NiSe heterostructures and mechanism discovery, ACS Catal. 13 (2022) 837–847.

[30] S. Ni, H. Qu, Z. Xu, X. Zhu, H. Xing, L. Wang, J. Yu, H. Liu, C. Chen, L. Yang, Interfacial engineering of the $NiSe_2/FeSe_2$ pp heterojunction for promoting oxygen evolution reaction and electrocatalytic urea oxidation, Appl. Catal. B: Environ. 299 (2021) 120638.

[31] J. Kang, Y. Xue, J. Yang, Q. Hu, Q. Zhang, L. Gu, A. Selloni, L.-M. Liu, L. Guo, Realizing two-electron transfer in Ni $(OH)_2$ nanosheets for energy storage, J. Am. Chem. Soc. 144 (2022) 8969–8976.

[32] C. Rong, X. Shen, Y. Wang, L. Thomsen, T. Zhao, Y. Li, X. Lu, R. Amal, C. Zhao, Electronic structure engineering of single-atom Ru sites via $Co-N_4$ sites for bifunctional pH-universal water splitting, Adv. Mater. 34 (2022) 2110103.

[33] J. Li, C. Hou, C. Chen, W. Ma, Q. Li, L. Hu, X. Lv, J. Dang, Collaborative interface optimization strategy guided ultrafine RuCo and MXene heterostructure electrocatalysts for efficient overall water splitting, ACS Nano (2023).

[34] K. Chang, D.T. Tran, J. Wang, K. Dong, S. Prabhakaran, D.H. Kim, N.H. Kim, J. H. Lee, Triphasic Ni_2P-Fe_2P-CoP heterostructure interfaces for efficient overall water splitting powered by solar energy, Appl. Catal. B: Environ. (2023) 123016.

[35] Y. Wang, X. Li, Z. Huang, H. Wang, Z. Chen, J. Zhang, X. Zheng, Y. Deng, W. Hu, Amorphous Mo-doped $NiS_{0.5}Se_{0.5}$ nanosheets@ crystalline $NiS_{0.5}Se_{0.5}$ nanorods for high current-density electrocatalytic water splitting in neutral media, Angew. Chem. Int. Ed. 62 (2023) e202215256.

[36] Y. Wang, X. Li, M. Zhang, J. Zhang, Z. Chen, X. Zheng, Z. Tian, N. Zhao, X. Han, K. Zaghib, Highly active and durable single-atom tungsten-doped $NiS_{0.5}Se_{0.5}$ nanosheet@ $NiS_{0.5}Se_{0.5}$ nanorod heterostructures for water splitting, Adv. Mater. 34 (2022) 2107053.

[37] H. Qin, W. Zhang, Q. Zheng, C. Li, X. Zhang, N. Li, P. Zhang, H. Bu, S. Zhang, X. Xu, Designed $CoSe_2@ ZnIn_2S_4$ large area 2D/2D Schottky junction for efficient photo-utilization hydrogen evolution and biomass oxidation, Chem. Eng. J. 477 (2023) 146947.

[38] K. Wu, C. Lyu, J. Cheng, Z. Guo, H. Li, X. Zhu, W.M. Lau, J. Zheng, Modulating electronic structure by etching strategy to construct $NiSe_2/Ni_{0.85}Se$ heterostructure for urea-assisted hydrogen evolution reaction, Small (2023) 2304390.

[39] H. Qin, Y. Ye, J. Li, W. Jia, S. Zheng, X. Cao, G. Lin, L. Jiao, Synergistic engineering of doping and vacancy in Ni $(OH)_2$ to boost urea electrooxidation, Adv. Funct. Mater. 33 (2023) 2209698.

[40] K. Zhang, C. Liu, N. Graham, G. Zhang, W. Yu, Modulation of dual centers on cobalt-molybdenum oxides featuring synergistic effect of intermediate activation and radical mediator for electrocatalytic urea splitting, Nano Energy 87 (2021) 106217.

[41] R. Qin, P. Wang, Z. Li, J. Zhu, F. Cao, H. Xu, Q. Ma, J. Zhang, J. Yu, S. Mu, Ru-incorporated nickel diselenide nanosheet arrays with accelerated adsorption kinetics toward overall water splitting, Small 18 (2022) 2105305.

[42] S. Anantharaj, S. Noda, M. Driess, P.W. Menezes, The pitfalls of using potentiodynamic polarization curves for tafel analysis in electrocatalytic water splitting, ACS Energy Lett. 6 (2021) 1607–1611.

[43] D. Li, W. Wan, Z. Wang, H. Wu, S. Wu, T. Jiang, G. Cai, C. Jiang, F. Ren, Self-derivation and surface reconstruction of Fe-doped Ni_3S_2 electrode realizing high-efficient and stable overall water and urea electrolysis, Adv. Energy Mater. 12 (2022) 2201913.

[44] D. Liu, H. Ai, J. Li, M. Fang, M. Chen, D. Liu, X. Du, P. Zhou, F. Li, K.H. Lo, Surface reconstruction and phase transition on vanadium–cobalt–iron trimetal nitrides to form active oxyhydroxide for enhanced electrocatalytic water oxidation, Adv. Energy Mater. 10 (2020) 2002464.

[45] H. Su, W. Zhou, W. Zhou, Y. Li, L. Zheng, H. Zhang, M. Liu, X. Zhang, X. Sun, Y. Xu, In-situ spectroscopic observation of dynamic-coupling oxygen on atomically dispersed iridium electrocatalyst for acidic water oxidation, Nat. Commun. 12 (2021) 6118.

[46] J.T. Ren, L. Chen, W.W. Tian, X.L. Song, Q.H. Kong, H.Y. Wang, Z.Y. Yuan, Rational synthesis of core-shell-structured nickel sulfide-based nanostructures for efficient seawater electrolysis, Small (2023) 2300194.

[47] Y. Gan, Y. Ye, X. Dai, X. Yin, Y. Cao, R. Cai, X. Zhang, Self-sacrificial reconstruction of MoO_{42}- intercalated NiFe LDH/Co_2P heterostructures enabling interfacial synergies and oxygen vacancies for triggering oxygen evolution reaction, J. Colloid Interface Sci. 629 (2023) 896–907.

[48] W. Chen, L. Xu, X. Zhu, Y.C. Huang, W. Zhou, D. Wang, Y. Zhou, S. Du, Q. Li, C. Xie, Unveiling the electrooxidation of urea: intramolecular coupling of the N− N bond, Angew. Chem. Int. Ed. 60 (2021) 7297–7307.

[49] P. Wang, X. Bai, H. Jin, X. Gao, K. Davey, Y. Zheng, Y. Jiao, S.Z. Qiao, Directed urea-to-nitrite electrooxidation via tuning intermediate adsorption on Co, Ge Co-doped Ni sites, Adv. Funct. Mater. (2023) 2300687.

[50] X. Gao, S. Zhang, P. Wang, M. Jaroniec, Y. Zheng, S.-Z. Qiao, Urea catalytic oxidation for energy and environmental applications, Chem. Soc. Rev. 53 (2024) 1552.

[51] Z. Ji, Y. Song, S. Zhao, Y. Li, J. Liu, W. Hu, Pathway manipulation via Ni, Co, and V ternary synergism to realize high efficiency for urea electrocatalytic oxidation, ACS Catal. 12 (2021) 569–579.